Nonequilibrium patterns in phase-separating ternary membranes

Jordi Gómez, Francesc Sagués, and Ramon Reigada
Departament de Química-Física, Universitat de Barcelona, Avda. Diagonal 647, 08028 Barcelona, Spain
(Received 17 February 2009; revised manuscript received 29 April 2009; published 27 July 2009)

We present a nonequilibrium approach for the study of a two-dimensional phase-separating ternary mixture. When the component that promotes phase separation is dynamically exchanged with the medium, the separation process is halted and actively maintained finite-size segregation domains appear in the system. In addition to this effect, already reported in our earlier work [J. Gómez, F. Sagués, and R. Reigada, Phys. Rev. E **77**, 021907 (2008)], the use of a generic Ginzburg-Landau formalism and the inclusion of thermal fluctuations provide a more dynamic description of the resulting domain organization. Its size, shape, and stability properties are studied. Larger and more circular and stable domains are formed when decreasing the recycling rate, increasing the mobility of the exchanged component, and the mixture is quenched deeper. We expect this outcome to be of applicability in raft phenomenology in plasmatic cell membranes.

DOI: 10.1103/PhysRevE.80.011920 PACS number(s): 82.39.−k, 82.40.Ck, 82.20.Wt

I. INTRODUCTION

Domain formation in multicomponent soft-matter systems is commonly associated with the existence of dissimilar affinities between the components. In equilibrium, emerging structures are characterized by a wavelength dictated exclusively by the competition between the different molecular interactions [1]. In contrast, nonequilibrium labile condensed systems may show actively maintained patterns whose length scale results from the competition of thermodynamic forces (molecular interactions) and kinetic parameters accounting for transport and relaxation processes [2]. Pattern formation in condensed soft matter out of equilibrium has attracted much attention in a broad variety of physical problems [3–6] and is becoming of much interest in the study of particular biological systems. In this context, cell membranes are a classical example of multicomponent and highly labile biological soft matter generally found under nonequilibrium conditions, in the presence of chemical reactions, mass transport, and energy flows. With this perspective, pattern formation in nonequilibrium multicomponent lipid membranes has been addressed in recent works [7–10].

More specifically, the study of nonequilibrium pattern generation in lipid mixtures that form bilayers is particularly relevant in relation to one of the emergent issues in biophysics: the raft model in cell membranes. According to this hypothesis, lipids in plasma membranes are distributed heterogeneously forming small domains, known as *rafts*, rich in cholesterol and saturated lipids, embedded in a medium mostly containing unsaturated lipids [11]. Such structures are endowed with membrane protein sorting properties and, as a consequence, with many biological functions [12,13]. Although some aspects of the raft phenomenology still remain controversial, it is accepted that the preferential packing of cholesterol and saturated lipids constitutes the thermodynamic driving force for raft formation [14,15]. On the other hand, structural and dynamic properties of raft organization are believed to be dynamically regulated by the cell state and the specific signals or stimulus that may modify such state [16–18]. The active nature of raft organization, therefore, prompts to account not only for the thermodynamics of the lipid mixture but also for the nonequilibrium aspects affecting the cell membrane, as the transport of its components across the bilayer.

This scenario has inspired some modelization schemes [19,20] and we have recently presented a proposal [21] that is completed and extended in this paper. In our original paper [21], we described the thermodynamics of the lipid mixture by using the regular solution theory and derived the kinetic equations for the compositional fields supplemented with a cholesterol recycling term. Here, instead, a more generic Ginzburg-Landau free-energy formulation is used, allowing a straightforward implementation in the kinetic equations of a term mimicking thermal fluctuations, absent in our original and the other mentioned approaches. Although the main conclusions are not altered, the inclusion of fluctuations improves the model results: the obtained nonequilibrium domain organization displays a more dynamic aspect (domains form, change their shape, break up, move, coalesce, etc. in contrast to the more *rigid* outcome in Ref. [21]) as it corresponds to a more realistic description of pattern formation in fluid phases of labile systems. Moreover, this allows us to study other aspects than domain average size, as the shape of the emerging structures, as well as their temporal stability that could be relevant in the biological context.

The aim of the present paper is to formulate and to study a general model for phase-separating ternary two-dimensional mixtures under the effect of the continuous recycling of one of the components. We pay special attention to the size, shape, and stability of the formed domains and how these properties are affected by both thermodynamic and transport system conditions. Despite its generic formulation and presentation, we expect this study to be of particular interest and applicability in the membrane raft issue. The paper is organized as follows. In Sec. II, the model approach is described and its kinetic equations are derived. The linear stability analysis of these equations is performed in Sec. III and their discretization is presented in Sec. IV. Numerical simulations are carried out and some representative results are shown in Sec. V for different recycling rates and molecular interactions and mobilities. The correspondence of the model results to biological facts is discussed in Sec. VI. We conclude with a brief summary in Sec. VII.

II. MODEL AND KINETIC EQUATIONS

We address the study of a two-dimensional ternary mixture where two of the components (A and B), being miscible down to a critical temperature, may undergo phase separation due to the inclusion of a third molecular species (C). Preferential affinity of C for one of the other two components (say A) "advances" their demixing at temperatures higher than the original critical temperature. In relation to model membranes, A, B and C stand, respectively, for saturated lipids, unsaturated lipids, and cholesterol. The energetic description of the system follows a Ginzburg-Landau approach based on two spatial and time-dependent compositional variables, $\phi(\vec{r},t)$ and $c(\vec{r},t)$. ϕ corresponds to the differential composition of A and B components in the A/B mixture ($\phi>0$ indicating predominance of A component), whereas c stands for the fraction of the third species C with respect to a maximum allowed concentration of this component in the mixture. According to these two scalar fields, the free-energy functional per molecule can be written as

$$\frac{f[\phi,c]}{k_BT}=\left(\frac{1}{2}-J\right)\phi^2+\frac{1}{12}\phi^4-G\phi c+4\left(c-\frac{1}{2}\right)^2+\frac{8}{3}\left(c-\frac{1}{2}\right)^4, \tag{1}$$

where T is the temperature, k_B stands for the Boltzmann constant, and the parameters J and G are determined by the interaction between the components in the mixture. The energetic description in Eq. (1) is introduced here as a generic phenomenological approach based on the typical Landau expansion in ϕ^2, ϕ^4, c^2, and c^4 terms, plus the simplest (linear) coupling between the two compositional order parameters. Although we want to keep the phenomenological and generic nature of the proposal, it has to be noticed that analogous free-energy expressions can be derived from the expansion of a regular solution free-energy expression [21] or from a coarse-graining procedure of a discrete Ising-like approach based on two interconnected lattices (see details in Ref. [15]). In any case, a connection between the interaction Landau parameters J and G and the microscopic interaction strengths can be established. Particularly, the parameter J corresponds to the interaction between A and B components ($J>0$ corresponds to preferential affinity for components of the same kind), whereas G stands for the differential interaction between A and B components with C molecules ($G>0$ corresponds to a preferential affinity between C and A components).

The free-energy functional of the whole system can be expressed as

$$\mathcal{F}[\phi,c]=N_0\int_S\left(f[\phi,c]+\frac{\gamma}{2}|\vec{\nabla}\phi|^2\right)ds, \tag{2}$$

where the integration is performed over the membrane area S and the number of molecules per unit area is represented by N_0. Line tension between A-rich and B-rich phases, γ, can be estimated from Cahn-Hilliard theory [22] as $\gamma\approx Jd_0^2$, where J is the typical interaction energy and d_0 is the characteristic interfacial width. Contribution of component C to the line tension is not considered for simplicity.

Once the energy of the system is determined, the kinetic evolution of the compositional fields is obtained by applying the constitutive relations from linear nonequilibrium thermodynamics leading to

$$\frac{\partial\phi}{\partial t}=M_\phi\nabla^2\mu_\phi+\xi_\phi(\vec{r},t), \tag{3}$$

$$\frac{\partial c}{\partial t}=M_c\nabla^2\mu_c-\rho(c-\bar{c})+\xi_c(\vec{r},t), \tag{4}$$

which obey the conservation laws $S^{-1}\int_S\phi(\vec{r},t)ds=\bar{\phi}$ and $S^{-1}\int_S c(\vec{r},t)ds=\bar{c}$, with $\bar{\phi}$ and $\bar{c}$ being the constant average values of the compositional variables. The kinetic coefficients M_ϕ and M_c stand for the molecular mobilities that have been considered here to be concentration independent. The chemical potentials, μ_i, are expressed as the functional derivatives of the free energy with respect to the corresponding compositional variables

$$\mu_\phi=\frac{\delta\mathcal{F}[\phi,c]}{\delta\phi},\quad \mu_c=\frac{\delta\mathcal{F}[\phi,c]}{\delta c}. \tag{5}$$

The second term of the kinetic equation (4) deserves special attention. As anticipated, in this paper, we are interested in the transient and dynamic structures that arise when phase separation is halted due to the continuous recycling of one of the components. The second term of the kinetic equation (4) accounts for a generic nonequilibrium exchange process of component C; the parameter ρ being the recycling frequency (units of inverse of time). This nonequilibrium term can be interpreted as a continuous and homogeneous intake flux of component C and its continuous release at a rate dependent of its local concentration [21]. The proposed term is the simplest way to introduce a unique time scale, ρ^{-1}, for the recycling process keeping a constant total amount of the C component in the system. Finally, the last contributions of kinetic equations (3) and (4) correspond to Gaussian white-noise terms representing thermal fluctuations, taken to have zero mean and correlation

$$\langle\xi_i(\vec{r},t)\xi_i(\vec{r}',t')\rangle=-2k_BTM_i\nabla^2\delta(\vec{r}-\vec{r}')\delta(t-t'). \tag{6}$$

In order to simplify the kinetic description, the diffusion coefficients for both compositional variables are defined as $D_i=M_ik_BTN_0$. From now on, the equations, variables, and model parameters will be represented in their dimensionless form. To do so, energy is expressed in k_BT units, length is scaled following $x\rightarrow\frac{x}{\sqrt{\gamma/J}}$, and time units are scaled to $t\rightarrow\frac{tJD_\phi}{\gamma}$. Namely, k_BT, d_0, and D_ϕ are fixed to 1 and $D_c\rightarrow D=D_c/D_\phi$. The dimensionless kinetic equations then read as

$$\frac{\partial\phi}{\partial t}=\nabla^2\left[(1-2J)\phi+\frac{1}{3}\phi^3-Gc-\gamma\nabla^2\phi\right]+\sqrt{\epsilon_\phi}\nu_\phi, \tag{7}$$

$$\frac{\partial c}{\partial t} = D\nabla^2\left[-G\phi + 8\left(c-\frac{1}{2}\right) + \frac{32}{3}\left(c-\frac{1}{2}\right)^3\right] - \rho(c-\bar{c}) + \sqrt{\epsilon_c}\nu_c, \tag{8}$$

where $\nu_i(\vec{r},t)$ is a random variable that follows a Gaussian distribution with correlation

$$\langle \nu_i(\vec{r},t)\nu_i(\vec{r}',t')\rangle = -\nabla^2\delta(\vec{r}-\vec{r}')\delta(t-t') \tag{9}$$

and noise intensities $\epsilon_\phi = 2/N_0$ and $\epsilon_c = 2D/N_0$.

Since we are particularly interested in lipid membranes containing cholesterol, we adjust the free-energy parameters accordingly. Based on the regular solution theory (see, for example, Ref. [23]), the parameters J and G are related to the lipid-lipid and cholesterol-lipid differential interactions, $\omega_{ll} = 4J$ and $\omega_{cl} = G$, respectively. Actually, ω_{ll} is defined as the difference between the interaction energy of a pair AB and the interaction energy of a pair AA (considered equal to the energy of a pair BB). ω_{cl} accounts for the energy cost of the formation of a BC pair (for simplicity considered equal to the energy gain of a pair AC). These parameters can be obtained from experiments with different lipid systems [24,25] and a reasonable estimation for our model (with generic saturated and unsaturated lipids) leads to $J \in (0.1, 0.35)$ and $G \in (1.5, 3)$ in k_BT energy units. With respect to the average membrane composition, we have chosen a 2:3 molar ratio of saturated/unsaturated lipids ($\bar{\phi} = -0.2$) and a 30% of cholesterol in the membrane, which may correspond to a plausible cell membrane composition [26]. Following a common lattice system to describe lipid and cholesterol mixtures (see, for example, Refs. [15,21]) based on a triangular lattice for the lipid mixture and a complementary hexagonal lattice for cholesterol molecules, the molar fraction for this latter component is $2\bar{c}/(1+2\bar{c})$. This corresponds to $\bar{c} = 0.214$ for the proposed 30% of cholesterol molar percentage.

III. LINEAR STABILITY ANALYSIS

We can foresee some qualitative results from the linear stability analysis of the kinetic equations. We test the linear stability of the stationary homogeneous solution $[\phi(\vec{r}) = \bar{\phi},\ c(\vec{r}) = \bar{c}]$ by introducing small wave perturbations $\delta\phi \exp[w(q)t + i\vec{q}\cdot\vec{r}]$ and $\delta c \exp[w(q)t + i\vec{q}\cdot\vec{r}]$ and linearizing Eqs. (3) and (4). This procedure determines the 2×2 linearization matrix $\mathcal{L}$,

$$\begin{pmatrix} \mathcal{L}_{11} + w(q) & \mathcal{L}_{12} \\ \mathcal{L}_{21} & \mathcal{L}_{22} + w(q) \end{pmatrix}\begin{pmatrix} \delta\phi \\ \delta c \end{pmatrix} = \begin{pmatrix} 0 \\ 0 \end{pmatrix}, \tag{10}$$

with coefficients

$$\mathcal{L}_{11} = q^2[(1-2J) + \bar{\phi}^2 + \gamma q^2],$$

$$\mathcal{L}_{12} = -Gq^2,$$

$$\mathcal{L}_{21} = -DGq^2,$$

$$\mathcal{L}_{22} = Dq^2\left[8 + 32\left(\bar{c}-\frac{1}{2}\right)^2\right] + \rho.$$

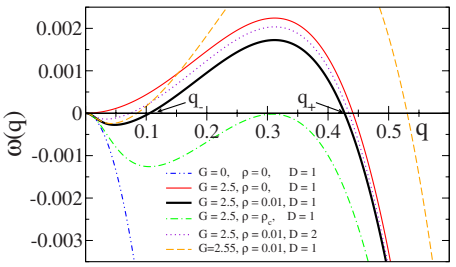

FIG. 1. (Color online) Growth rate $w(q)$ for different parameter values. For all curves, $J=0.25$, $\gamma=0.25$, $D=1$, $\bar{\phi}=-0.2$, and $\bar{c}=0.214$. The case with $\rho=0$ and $G=0<G_{c,eq}=2.394$ corresponds to miscibility. When G is increased above its critical value ($G=2.5>G_{c,eq}=2.394$, $\rho=0$), equilibrium phase separation is predicted. When a moderate recycling rate is applied ($G=2.5$, $\rho=0.01$), unstable modes appear at $q\in(q_-,q_+)$ leading to finite-size domains. Faster recycling increases the value of the minimum unstable mode $q-$, thus smaller domains are expected. If $\rho>\rho_c=0.045$, unstable modes become stable and the miscibility of the mixture is recovered. Larger diffusion parameter D (compare curves for $D=1$ and $D=2$) and/or larger interaction parameter G (compare curves for $G=2.5$ and $G=2.55$) decrease the value of q_-, so that larger domains are expected.

The growth rate $w(q)$ of the perturbations is calculated as the largest eigenvalue of the Jacobian resulting from the linearization matrix. The solutions of the eigenvalue problem are given by $w(q) = -\frac{1}{2}(\mathcal{L}_{11}+\mathcal{L}_{22}) \pm \frac{1}{2}\sqrt{(\mathcal{L}_{11}-\mathcal{L}_{22})^2 + 4\mathcal{L}_{12}\mathcal{L}_{21}}$.

In the absence of recycling process ($\rho=0$), the system evolves to two possible equilibrium states depending on the specific parameter values. For weak-interaction parameters, the system remains stable to small perturbations and no phase separation is observed. In this case, all modes have negative growth rates $w(q)<0\,\forall\, q>0$ except $w(q=0)=0$ (see Fig. 1). When the interaction parameters are above their critical values, large wavelength modes become unstable, promoting complete phase separation; namely, there exists a range of $q\in(0,q_0)$ where $w(q)>0$, whereas $w(q)<0$ for $q\in(q_0,\infty)$ (see Fig. 1). In this situation, the equality $w(q)=0$ is fulfilled, $q=0$ and $q=q_0$ that follows

$$q_0^2 = -\frac{\bar{\phi}' - 2J}{\gamma} + \frac{G^2}{16\bar{c}'\gamma}, \tag{11}$$

where $\bar{\phi}' = 1+\bar{\phi}^2$ and $\bar{c}' = 1+2\bar{c}(\bar{c}-1)$. The expression for q_0 can be used to determine the critical values in equilibrium conditions, $J_{c,eq,\mathrm{AB}}$ and $G_{c,eq}$. In the absence of component C, $q_0^2>0$ only holds if $J>J_{c,eq,\mathrm{AB}}$, where

$$J_{c,eq,\mathrm{AB}} = \frac{\bar{\phi}'}{2}. \tag{12}$$

If component C is added to the system, equilibrium phase separation occurs for $J<J_{c,eq,\mathrm{AB}}$ when $G>G_{c,eq}$ and

$$G_{c,eq} = 4\sqrt{2(J_{c,eq,\mathrm{AB}} - J)\bar{c}'}. \tag{13}$$

The scenario studied in this paper corresponds to a miscible binary A/B mixture ($J<J_{c,eq,\mathrm{AB}}$) than undergoes phase sepa-

ration due to the inclusion of a third component C, $G > G_{c,eq}$.

In nonequilibrium conditions and moderate recycling rates, the equality $w(q)=0$ holds at $q=0$, q_-, and q_+. In this situation, a range of unstable modes, $w(q)>0$, appears at intermediate wave numbers $q \in (q_-, q_+)$ (see Fig. 1). This means that the phase separation process evolves until segregating domains reach a maximum size, L, determined by the smallest unstable wave number: $L \sim \pi/q_-$. Larger domains are not attainable since the corresponding modes are stable, $w(q<q_-)<0$. This outcome of the linear stability analysis is a reflection of the competition between thermodynamic ordering and nonequilibrium mixing actions. In the absence of recycling, phase separation would evolve up to equilibrium; namely, to the complete segregation of the system into two separated phases. However, the transport across the bilayer of the component that promotes phase separation affects the segregation process introducing a long-range mixing effect that competes with the short-range ordering thermodynamic action and eventually prevents complete phase separation. As a result, actively maintained finite-size segregation domains appear in the system, their properties being regulated by the balance between the thermodynamic and transport applied conditions.

The analytical determination of q_- provides, therefore, an upper limit for the size of nonequilibrium domains in the stationary state and its dependence on the model parameters. The analytical expressions for q_- and q_+ read

$$q_{\pm}^2 = \frac{(J_{c,eq,\mathrm{AB}} - J)}{\gamma}\left(\mathcal{A} \pm \sqrt{\mathcal{A}^2 - \frac{4\gamma\rho}{DG_{c,eq}^2}}\right), \tag{14}$$

where

$$\mathcal{A} = \frac{D(G^2 - G_{c,eq}^2) - \gamma\rho}{DG_{c,eq}^2}. \tag{15}$$

Equation (14) can be used to predict how the maximum domain size depends on the rest of the parameters of the model. However, the dependence of q_- with the rest of the parameters in Eq. (14) is not very handy. Instead, we use a simpler approach that will be useful in the forthcoming discussions. For $q_- \ll 1$, the q^4 factor in $\mathcal{L}_{11}$ can be neglected and a simpler version of Eq. (14) is found

$$q_-^2 \approx \frac{\rho(\bar{\phi}' - 2J)}{D(G^2 - 16(\bar{\phi}' - 2J)\bar{c}')} = \frac{2\rho(J_{c,eq,\mathrm{AB}} - J)}{D(G^2 - G_{c,eq}^2)}. \tag{16}$$

Notice that two important aspects can be extracted from the latter expression. First, Eq. (16) predicts that q_-^2 is proportional to ρ; namely, the faster recycling rate, the smaller the predicted maximum size for nonequilibrium structures. Second, the deeper the mixture quench (larger J and/or G interaction parameters), the larger domain predicted size. The opposite effect of recycling rate and quench depth in Eq. (16) accounts for the competition between nonequilibrium and thermodynamic forces, respectively, commented along this paper.

By looking at Eq. (16) in more detail, additional findings can be noticed. For example, when the binary A/B mixture is placed far from its phase boundary ($J \ll J_{c,eq,\mathrm{AB}}$), domains are predicted to be small. Furthermore, smaller values for the diffusion parameter D also result in smaller nonequilibrium structures. Summing up, small domains are obtained when the recycled component in the mixture is the one with the largest differential interaction strength and the one with smaller mobility.

When the recycling rate is higher than a critical value ρ_c, $w(q)=0$ is only fulfilled at $q=0$ and all positive wavenumber modes are stable, $w(q>0)<0$. In this situation, the nonequilibrium recycling process is so fast that the system is kinetically kept miscicle. The critical value ρ_c can be obtained from the equality $q_-=q_+$ (see Fig. 1). This means that the critical value ρ_c is one of the solutions of the equation $\mathcal{A}^2 = \frac{4\gamma\rho}{DG_{c,eq}^2}$, leading to

$$\rho_c = \frac{D}{\gamma}(G_{c,eq} - G)^2. \tag{17}$$

IV. SIMULATION DETAILS AND UNITS

The differential kinetic Eqs. (3) and (4) are numerically solved in a two-dimensional square lattice of $N \times N$ sites for the compositional fields ϕ and c. Periodic boundary conditions are applied. The discretization mesh size is chosen to be of the order of the characteristic interfacial width d_0 and set to $\Delta x=1$, whereas the time step is set to $\Delta t=0.001$. Both choices assure a good numerical convergence. Simulations are started from a homogeneous distribution $[\phi(\vec{r},0) = \bar{\phi},\ c(\vec{r},0)=\bar{c}]$ slightly perturbed with local variations of $\pm 1\%$. The discretized kinetic equations are

$$\phi_{i,j}^{k+1} = \phi_{i,j}^k + \frac{\Delta t}{2\Delta x^2}\nabla_{i,j}^2\left[(1-2J)\phi_{i,j}^k + \frac{1}{3}\phi_{i,j}^{k\,3} - \frac{\gamma}{\Delta x^2}\nabla_i^2\phi_{i,j}^k - Gc_{i,j}^k\right] + \sqrt{\epsilon_\phi \frac{\Delta t}{\Delta x^2}}\vec{\nabla}_{i,j}\vec{v}_{\phi,i,j}^k, \tag{18}$$

$$c_{i,j}^{k+1} = c_{i,j}^k + \frac{\Delta t}{2\Delta x^2}\nabla_i^2\left[-Gc_{i,j}^k + 8\left(c_{i,j}^k - \frac{1}{2}\right) + \frac{32}{3}\left(c_{i,j}^k - \frac{1}{2}\right)^3\right] + \sqrt{\epsilon_c \frac{\Delta t}{\Delta x^2}}\vec{\nabla}_{i,j}\vec{v}_{c,i,j}^k. \tag{19}$$

The compositional fields are defined in the sites $i,j \in [1,N]$. The temporal integration is performed by successively iterating the discretized kinetic equations, with k being the corresponding iteration index. The total time lapse up to iteration k is then $t=k\Delta t$. The discretized Laplacian operator is defined for a generic function y as

$$\nabla_{i,j}^2 y_{i,j} = y_{i+1,j} + y_{i-1,j} + y_{i,j+1} + y_{i,j-1} - 4y_{i,j}. \tag{20}$$

The discretized divergence operator applied on the noise vector $\vec{v}_{i,j}=(v_{i,j}^{(1)}, v_{i,j}^{(2)})$ reads

$$\vec{\nabla}_{i,j}(v_{i,j}^{(1)},v_{i,j}^{(2)}) = \frac{v_{i+1,j}^{(1)} - v_{i-1,j}^{(1)}}{2} + \frac{v_{i,j+1}^{(2)} - v_{i,j-1}^{(2)}}{2}, \quad (21)$$

being $\nu^{(1)}$ and $\nu^{(2)}$ independent Gaussian random variables generated every iteration at each lattice site. This expression fulfills the fluctuation-dissipation relation for the thermal noise in the discretized kinetic equations.

For the case of lipid membranes, we choose d_0 of the order of a few lipid molecular distances in the membrane plane, $d_0 \approx 5$ nm. Since we have chosen $\Delta x = d_0$ and according to usual lipid membrane areas per molecule, each discretization site contains about 50 molecules, validating the coarse-grained nature of the compositional order parameters. The choice of $\Delta x = 1$ fixes the simulation length units to 5 nm. The time simulation units can be extracted from the value of the diffusion coefficient. Since $D_\phi = 1$ and for a generic membrane lipid molecule in a bilayer the diffusivity is of the order of $\mu m^2/s$ [26], this implies $\Delta t = 2.5 \times 10^{-8}$ s. Simulations in this paper are performed in lattices of $N = 256$ up to 10^8 iterations that correspond to 1.28×1.28 μm^2 systems simulated for 2.5 s.

V. NUMERICAL RESULTS

One of the aims of this paper is to analyze the structural and dynamic characteristics of the domains that are formed when the mixture is quenched and maintained out of equilibrium by the recycling process. We are interested in the size, shape, and stability of those domains and how those features correlate with the different parameters of the model. The basic tools used to determine domain boundaries, size, roughness, and stability are described here.

Correlation functions are common numerical instruments to quantify characteristic time and length scales in pattern formation phenomena. The stability of domains can be estimated by computing the temporal correlation function once the system has already reached its stationary state. The normalized temporal correlation function for the ϕ field reads

$$T(\tau) = \frac{\langle \phi(\vec{r},t)\phi(\vec{r},t+\tau)\rangle - \langle \phi(\vec{r},t)\rangle^2}{\langle \phi(\vec{r},t)^2\rangle - \langle \phi(\vec{r},t)\rangle^2}, \quad (22)$$

where the brackets stand for an average over positions $\vec{r}$ and time t. Stable domains are identified by temporal correlation functions that hardly decay with time, whereas transient and highly dynamic structures yield to temporal correlation functions that quickly drop to zero. In order to monitor the spatial pattern evolution, we compute the normalized spatial correlation function for each compositional variable at different times. The normalized correlation function for the ϕ variable reads

$$C(\vec{r},t) = \frac{\langle \phi(\vec{r}',t)\phi(\vec{r}'+\vec{r},t)\rangle - \langle \phi(\vec{r}',t)\rangle^2}{\langle \phi(\vec{r}',t)^2\rangle - \langle \phi(\vec{r}',t)\rangle^2}, \quad (23)$$

where the brackets correspond to an average over positions $\vec{r}'$. An usual estimation for the characteristic length of the developed patterns at time t is given by the smallest distance $r=R$ that satisfies $C(R,t)=0$. We can define analogous time and spatial correlation functions for the c field.

A more detailed characterization of the stationary domains is provided by the following additional analysis that takes into account the presence of thermal fluctuations. First, thermal noise level is quantified as the standard deviation of the compositional fields in a simulation without interaction between the system components ($J=G=0$). Segregating domains are then defined as all interconnected lattice sites with a composition variable 3 times larger than the noise level. Once the domains have been delimited, domain area distribution histograms and mean domain linear sizes, $L=\sqrt{\text{area}}$, can be computed. Another feature that can be analyzed with this procedure is the roughness of the emerging domains. Particularly, the roughness index of a domain $i(\Omega_i)$ is computed as the square of the ratio between the perimeter of the domain (P_i) and the perimeter of the equivalent circle with the same area (A_i), $\Omega_i = \frac{P_i^2}{4\pi A_i}$. A circular domain has a roughness index $\Omega = 1$ whereas more irregular structures are characterized by $\Omega \gg 1$.

A. Role of the recycling frequency

Numerical simulations follow the predictions of the linear stability analysis. First, we analyze the effect of the parameter ρ. Two sets of simulations varying the recycling frequency have been performed for simulations with $\bar{\phi} = -0.2$, $\bar{c} = 0.214$, $J = 0.25$, $\gamma = 0.25$, and $D = 1$: $\rho = 0.001$, 0.005, 0.01, 0.02, and 0.04 for $G = 2.5$ and $\rho = 0.005$, 0.01, 0.02, 0.04, and 0.15 for $G = 3$. All these attempted recycling frequencies are smaller than the value of the corresponding ρ_c. The temporal evolution of the characteristic length R computed from the spatial correlation functions is presented in Fig. 2. The simulations that do not consider recycling (equilibrium phase separation) display a continuous pattern growth, whereas in most nonequilibrium cases ($\rho \neq 0$), a stabilization of the pattern to a stationary length is observed. Only the cases with very slow recycling still display domain growth at late times, which means that the stationary state has not been already achieved. As an example to illustrate pattern evolution, in Fig. 3, we present some pattern snapshots of the numerical simulations for the case $G = 2.5$ and different recycling rates. Observe, as a general behavior, how the system is segregated in coarsening domains and how the coarsening process is halted at smaller structures as the recycling frequency is increased.

Analysis of the occurrence area and roughness histograms gives more specific information on the structure of the stationary domains and its dependence on the exchange rate ρ. The domain area distributions have been computed for the last snapshots of each simulation (stationary state) and have been plotted in Fig. 4. It is observed that for a given interaction G, the average domain area diminishes as it also does its dispersion when the exchange process is made faster. The stationary mean domain size, L_{st}, corresponds to the square root of the mean domain area computed for each area distribution and their values depend, as expected, on the applied exchange rate applied. Particularly, larger ρ favors smaller domains. A plot of the inverse of the stationary sizes $1/L_{st}$ is presented in Fig. 5 as a function of $\rho^{1/2}$. Notice that the prediction in Eq. (16) is clearly fulfilled by our numerical

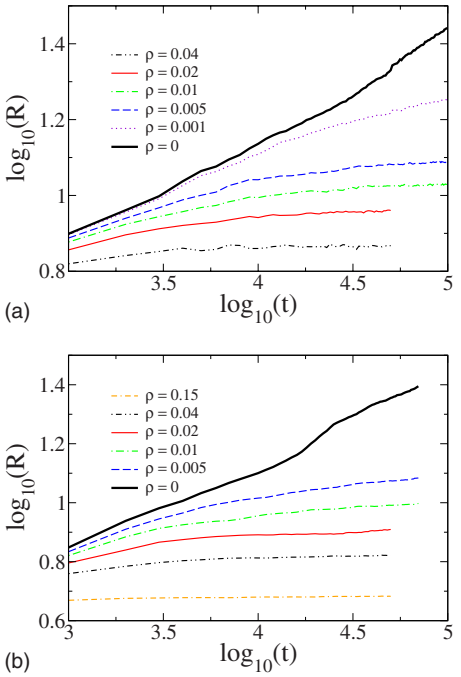

FIG. 2. (Color online) Log-log temporal evolution of characteristic length, R, for different recycling rates. The other parameters are $\bar{\phi}=-0.2$, $\bar{c}=0.214$, $D=1$, $\gamma=0.25$, and $J=0.25$. (a) $G=2.5$. (b) $G=3$. Each curve is computed as the average over three simulations obtained from different initial random distributions.

simulations with respect to the dependence on $\rho(q_- \propto \rho^{1/2})$. Only the cases with the largest ρ values seem to slightly deviate from the linear behavior. This can be understood since the larger the ρ, the larger the q_-, whereas $q_- \ll 1$ is assumed in Eq. (16). With respect to the domain roughness, increasing ρ results in rougher domains (see the insets in Fig. 4).

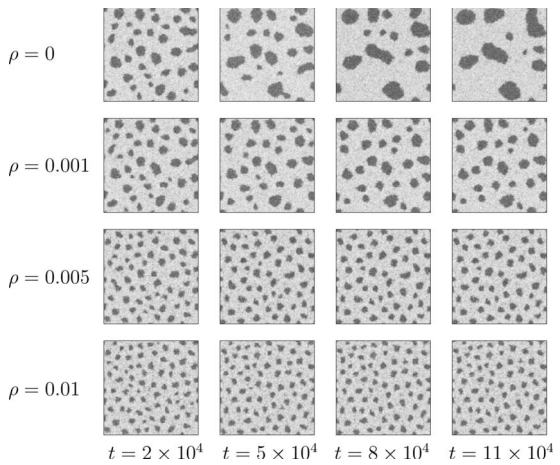

FIG. 3. Temporal evolution of the simulation patterns in a 256 $\times$256 system for different recycling rates. The other parameters are $\bar{\phi}=-0.2$, $\bar{c}=0.214$, $D=1$, $\gamma=0.25$, $J=0.25$, and $G=2.5$. Each snapshot corresponds to a grayscale representation of the parameter ϕ. Darker regions correspond to higher values of this variable. The snapshots for c follow the same distribution (not shown). Only the last snapshots for the nonequilibrium cases ($\rho \neq 0$) are practically stationary.

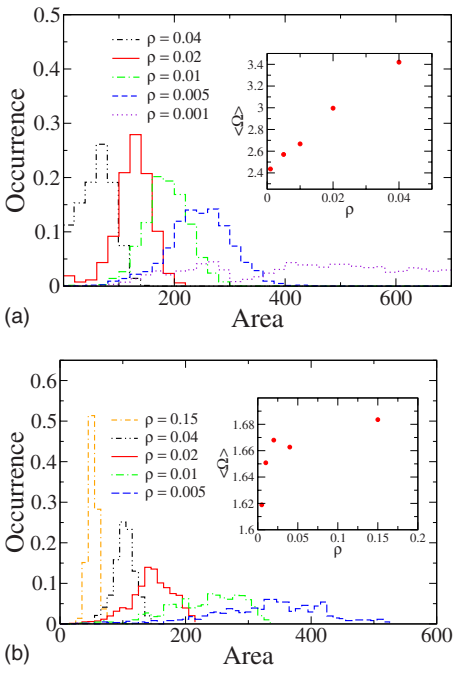

FIG. 4. (Color online) Domain area distributions for different values of ρ. (a) $G=2.5$. (b) $G=3$. The values of the other parameters are $\bar{\phi}=-0.2$, $\bar{c}=0.214$, $\rho=0.02$, $D=1$, $\gamma=0.25$, and $J=0.25$. Inset: mean roughness coefficient $\langle\Omega\rangle$ as a function of ρ.

The stability of the generated domains is analyzed by means of the temporal correlation functions plotted in Fig. 6 for different values of ρ. It is clearly observed how faster recycling rates make domains become less stable. In summary, for a given set of parameters, the effect of increasing the recycling frequency favors the generation of monodisperse small, irregular, and unstable domains, whereas slow recycling forms polydisperse large, rounded, and stable structures. Simulations also show how the system can dynamically adapt its lateral organization to changes in the speed of the exchange process. A system that is successively simulated under different recycling rates adjusts accordingly its lipid distribution [27]. For example, if recycling is absent, domains grow up to complete phase separation. At this point,

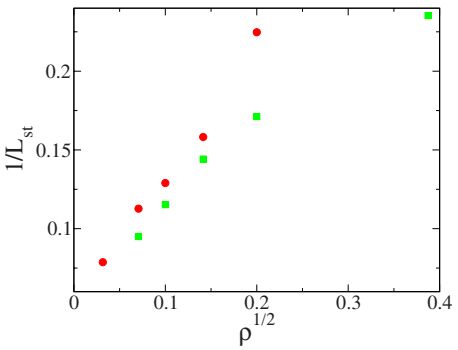

FIG. 5. (Color online) Inverse of the stationary domain linear size $1/L_{st}$ as a function of $\rho^{1/2}$ for $G=2.5$ (circles) and $G=3$ (squares). The other parameters are $\bar{\phi}=-0.2$, $\bar{c}=0.214$, $D=1$, $\gamma=0.25$, and $J=0.25$. The linear dependence predicted in Eq. (16) is captured.

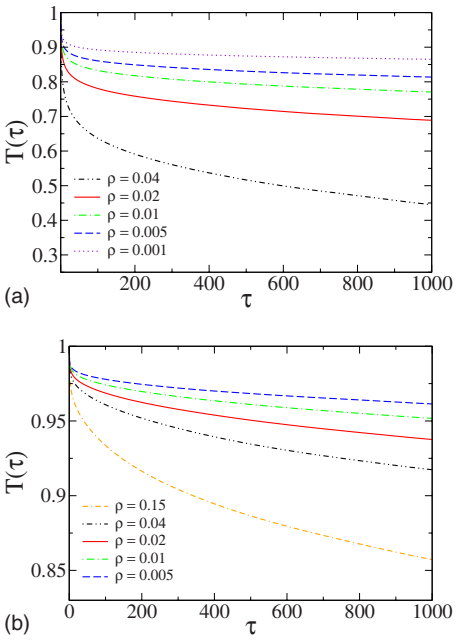

FIG. 6. (Color online) Decay of time-correlation functions for different values of ρ. (a) $G=2.5$. (b) $G=3$. The values of the other parameters are $\bar{\phi}=-0.2$, $\bar{c}=0.214$, $D=1$, $\gamma=0.25$, and $J=0.25$.

if fast recycling is applied, small and transient domains are recovered [27].

A final consideration has to be done with respect to the cases with a high recycling rate $\rho > \rho_c$. In this situation, numerical simulations without thermal fluctuations result in an homogeneous final distribution for the compositional variables ϕ and c, as it is predicted by the linear stability analysis (all modes are stable). However, the presence of thermal fluctuations on the kinetic equations may lead to the formation of very small and unstable domains in the numerical simulations. The size and stability of these structures, however, may be of relevance when ρ, although larger, is close to the critical value ρ_c. In this case, certain modes of the order of $q=q_-=q_+$ are only slightly stable and therefore can be eventually and locally excited by thermal fluctuations leading to domains with a significant size and stability [28]. This scenario will be addressed in more detail in a future work.

B. Modifying the thermodynamic conditions

The effects of modifying the thermodynamic conditions (namely, changes in the distance to the phase boundary of the mixture) are analyzed by varying the interaction energy G while keeping constant the remaining parameters. This analysis can be performed by comparing the data for $G=2.5$ and $G=3$ in former Figs. 2 and 4–6 at equal values of ρ. Doing so, it is observed that an increment of the interaction energy G (namely, a deeper mixture quench) results in larger, more circular, and more stable domains. Contrarily, when the separating mixture is closer to the phase boundary (smaller value of G, but still larger than $G_{c,eq}$), the mixing effect due to the exchange process makes the domains smaller and more irregular and unstable. The competition between thermodynamics and nonequilibrium is again visualized with this comparison and the prediction of the linear stability analysis in Eq. (16) is also captured in the numerical simulations.

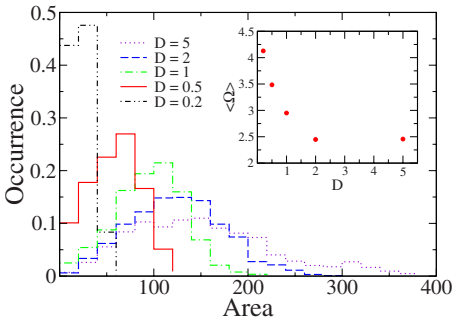

FIG. 7. (Color online) Size distribution of clusters for different values of the diffusion parameter D. The remaining parameters are $\bar{\phi}=-0.2$, $\bar{c}=0.2142$, $\rho=0.02$, $J=0.25$, and $G=2.5$. Inset: mean roughness coefficient $\langle\Omega\rangle$ as a function of D.

C. Effect of diffusion coefficient

Finally, the effect of the diffusion parameter is discussed. The parameter D was defined as the relative diffusivity of the C component respect to that of the A and B species ($D=D_c/D_\phi$). We have run simulations for $D=0.2$, 0.5, 1, 2, and 5, fixing $\rho=0.02$, $\bar{\phi}=-0.2$, $\bar{c}=0.214$, $\gamma=0.25$, $J=0.25$, and $G=2.5$. Area domain distributions and domain roughness are plotted in Fig. 7 and the behavior of the stationary domain linear size is presented in Fig. 8. From these figures, it is clear that larger D favors larger [as predicted in Eq. (16)] and more rounded domains. Moreover, increasing D also results in more stable domains as it can be observed in Fig. 9 where the time-correlation functions are shown. Actually, the effect of D is analogous to that of G in the previous section. Notice that the case of $D=0.2$ corresponds to the situation commented above where the system is dynamically kept miscible ($G > G_{c,eq}$ and $\rho > \rho_c$) but thermal fluctuations lead to domains with a significant size and stability [28].

VI. SPECULATIONS ON THE CORRESPONDENCE TO RAFT PHENOMENA

As anticipated, the proposed model and its results may be of interest in the study of raft formation in plasmatic cell membranes. Rafts correspond to lipid liquid-ordered nan-

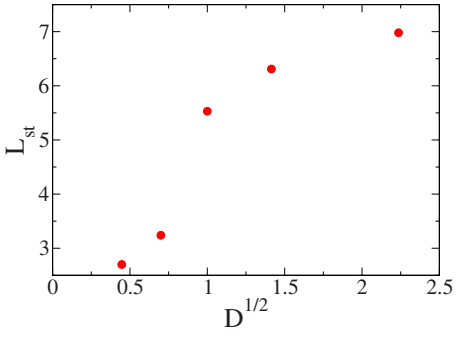

FIG. 8. (Color online) Stationary domain linear size L_{st} as a function of $D^{1/2}$. The other parameters are $\bar{\phi}=-0.2$, $\bar{c}=0.214$, $\rho=0.02$, $J=0.25$, and $G=2.5$.

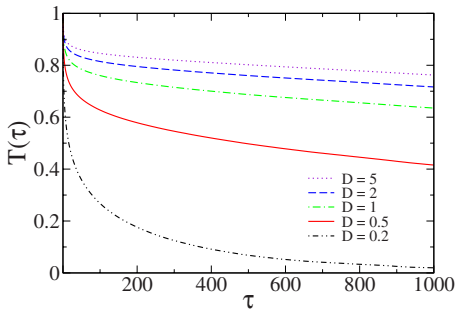

FIG. 9. (Color online) Decay of time-correlation functions for different values of the diffusion parameter D. The remaining parameters are $\bar{\phi}=-0.2$, $\bar{c}=0.214$, $\rho=0.02$, $J=0.25$, and $G=2.5$.

odomains rich in saturated lipids and cholesterol, *floating* in a liquid-disordered phase rich in unsaturated lipid species. Recent experiments [16,17] have revealed that raft organization is extremely sensitive to cholesterol homeostasis. Cholesterol is continuously incorporated into the membrane from the endoplasmatic reticulum and released to the external circulation [31]. According to this scenario, the lipid mixture phase-separates due to the presence of cholesterol that, in turn, is dynamically recycled or exchanged with the membrane environment. Therefore, raft formation may fit the scenario described with our model.

However, some caution must be exercised when comparing the spatial and temporal scales of the numerical examples provided in this paper so far. For instance, the case with $G=2.5$ in Fig. 5 leads to nonequilibrium domains of ≈ 62.5 nm for $\rho=40$ s^{-1} and ≈ 38.5 nm for $\rho=400$ s^{-1}. Both size values are in good agreement with the typical raft characteristic lengths, but the estimations of the values for the recycling frequencies are much larger than the biological values (of the order of s^{-1}) [32]. Despite this discrepancy, we also showed that similar small domain sizes could be attained for smaller recycling frequencies if the mixture were placed closer enough to the phase boundary and, actually, this is the accepted situation for lipid mixtures in cell membranes [16]. Therefore, our model may fit raft formation phenomena in the limit of close proximity to the phase boundary.

It has to be noticed also that the formulation of the model has been presented so far from a general viewpoint, so that in order to approach the biological context of raft formation in cell membranes, some particular aspects have to be taken into account. First, the fact that membrane components have a mobility that depends on the ordered nature of the lipid phase where they reside. On this respect, lipid mobilities can be up to 10 times larger in the liquid-disordered phase (poor in cholesterol) than in the liquid-ordered phase that forms raft domains (rich in cholesterol). To incorporate this particularity of the biological context, one may use lipid and cholesterol diffusivities that depend on the cholesterol composition in a simple functional manner such as

$$D_\phi(c) = \frac{D_{\phi,0}}{1+\Lambda c}, \quad D_c(c) = \frac{D_{c,0}}{1+\Lambda c}. \tag{24}$$

This choice implies that the diffusion constant of a lipid or cholesterol molecules is $1+\Lambda$ times smaller in a fully ordered phase (maximum cholesterol concentration $c=1$) than in a disordered phase ($c=0$). The linear stability analysis of the kinetic equations once this modification is considered leads to a correction for the smallest unstable wave number q_- in Eq. (16) that replaces the parameter D by $\frac{D}{1+\Lambda\bar{c}}$ (where D is again the fraction of cholesterol and lipid diffusion coefficients $D_{c,0}/D_{\phi,0}$). So, this correction goes in favor of the formation of smaller steady-state domains.

Another improvement to be considered is a more realistic description of the cholesterol transport across the membrane. The recycling contribution in Eq. (4) corresponds to the simplest generic choice to introduce a nonequilibrium mass transport process in the kinetic equations, but it does not fully describe the real biology of the cholesterol transport through a living cell membrane. Although what we call the "real biology" of the problem is rather complicated and still far from being understood, a strong simplification indicates that cholesterol intake involves the fusion to the membrane of small cholesterol-rich liposomes from its cytoplasmatic side, whereas efflux of cholesterol mainly takes place by the release of single sterol molecules to externally circulating lipoproteins [31]. Therefore, on what respects to the cholesterol influx, we should consider the incorporation of small pieces of the membrane instead of the proposed homogeneous cholesterol influx. We have to admit, however, that our continuum approach does not allow such possibility and is only correct in the limit of sufficiently small intake liposomes. A proposal that considers the exchange of membrane pieces has been presented by Turner *et al.* in Ref. [20], whose approach follows a purely temporal aggregation scheme without spatial resolution, quite different from ours but rather complementary. With respect to cholesterol efflux, a limitation of the generic formulation in Eq. (4) is that the cholesterol release frequency is constant (ρ). In a lipid membrane, cholesterol is more bound to the membrane in the ordered regions where cholesterol is abundant, so it is expected that the release frequency of this component has to be smaller in cholesterol-rich domains. To account for this effect, we may consider the following transport terms in Eq. (4):

$$\dot{c} = \cdots + \rho_{in} - \rho_{out}(c)c + \cdots, \tag{25}$$

where ρ_{in} is the cholesterol influx rate and $\rho_{out}(c)$ is an efflux frequency that depends on the cholesterol composition in a simple functional manner such as

$$\rho_{out}(c) = \frac{\rho_0}{1+\Psi c}. \tag{26}$$

This choice implies that the release frequency is $1+\Psi$ times smaller in a fully ordered phase (maximum cholesterol concentration $c=1$) than in a disordered phase ($c=0$). The linear stability analysis of the kinetic equations once this modification is considered leads to a correction for the smallest unstable wave number q_- in Eq. (16) that replaces the parameter ρ by $\frac{\rho_0}{(1+\Psi\bar{c})^2}$, where now $\bar{c}=\frac{\rho_{in}}{\rho_0-\rho_{in}\Psi}$. So, this correction goes in favor of the formation of larger steady-state domains. Summing up the two effects, one has that the corrected expression for the smaller unstable wave number q_- that pre-

dicts the maximum size of the steady-state domains reads

$$q_-^2 \approx \frac{2\rho_0(1+\Lambda\bar{c})(J_{c,eq,\mathrm{AB}}-J)}{D(1+\Psi\bar{c})^2(G^2-G_{c,eq}^2)}. \quad (27)$$

A simple estimation for a decrease of up to 10 times of both mobilities and efflux frequency when going from $c=0$ to $c=1$ results in a predicted size for the nonequilibrium domains 1.7 times larger than without the corrections, so still in the same length scale. In any case, we remind here that conditions of application of the proposal (independently of the improved descriptions of mobilities and cholesterol fluxes introduced in the latter paragraph) are always limited to the case of sufficiently close proximity to the miscibility boundary. The intrinsic simplicity of the model scheme does not allow stating a more general applicability.

Despite these considerations, our model results are consistent with a hierarchical picture of an active lipid organization at different length scales that are exploited for distinct functions [33,34]. The existence of small, transient lipid ordered domains may induce short-lifetime protein interactions necessary to facilitate specific biochemical reactions in the membrane. Larger and stabilized rafts, resulting from the coalescence of small and temporary domains, may be required for protein trafficking, endocytosis, and signaling. Such picture requires taking into account the dynamic nature of lipid domains that may dynamically change under specific signals or stimulus, contributing to the diversification of cellular responses [16–18].

Also in the context of biomembranes, a similar effect due to integral proteins has been suggested to regulate the size of segregated lipid domains [35–37]. The idea is based on the fact that the presence of active inclusions in a binary separating mixture reorganizes its spatial configuration by maintaining a steady-state organization in finite-size domains [35,36]. Such active impurities can be viewed as on/off proteins inserted in a separating lipid mixture, where activated and deactivated proteins prefer a particular lipid component. Analogously to our proposal, the rate of protein conversion determines the size of the steady-state domains [37].

VII. SUMMARY

We have presented the study of a nonequilibrium model for a ternary phase-separating mixture in a two-dimensional system where the component that promotes phase separation is continuously recycled. In this scenario, nonequilibrium recycling process halts the segregation of components and leads to the formation of finite-size domains. In this paper, the approach presented in our earlier work [21] has been completed and expanded with the inclusion of thermal fluctuations that provide a more dynamic picture. In the stationary state, domains form, diffuse, break up, and coalesce. We have analyzed not only the size but the shape and stability of the segregating structures as a function of the thermodynamic conditions of the mixture and the kinetics of the transport processes acting on it.

Our main conclusions can be summarized as follows. Increasing the recycling rate, decreasing the mobility of the exchanged component, and approaching the mixture to its phase boundary act in the same direction: domains become smaller, more irregular, and less stable. In the opposite situations, larger, more circular, and more stable domains are formed. We have also identified situations where even in the absence of phase separation, thermal fluctuations promote a certain organization in very small, irregular, and short-lived domains. This observation could be connected to the NMR detection of very small and transient domains in miscible ternary lipid vesicles [29,30] and will be addressed in more detail in a future work. Finally, the application of the model to the study of raft formation in the plasmatic cell membrane has been discussed and we have concluded that our model results may fit raft phenomena if the studied lipid mixture is in the limit of close proximity to the miscibility boundary.

ACKNOWLEDGMENTS

Partial support was provided by SEID through Project No. FIS200603525 and by DURSI through Project No. 2005-SGR000653.

[1] M. Seul and D. Andelman, Science **267**, 476 (1995).
[2] A. S. Mikhailov and G. Ertl, Science **272**, 1596 (1996).
[3] S. C. Glotzer, E. A. Di Marzio, and M. Muthukumar, Phys. Rev. Lett. **74**, 2034 (1995).
[4] Q. Tran-Cong and A. Harada, Phys. Rev. Lett. **76**, 1162 (1996).
[5] J. Verdasca, P. Borckmans, and G. Dewel, Phys. Rev. E **52**, R4616 (1995).
[6] M. Hildebrand, A. S. Mikhailov, and G. Ertl, Phys. Rev. Lett. **81**, 2602 (1998).
[7] J.-B. Manneville, P. Bassereau, D. Lévy, and J. Prost, Phys. Rev. Lett. **82**, 4356 (1999).
[8] P. G. Petrov, J. B. Lee, and H.-G. Döbereiner, Europhys. Lett. **48**, 435 (1999).
[9] R. Reigada, J. Buceta, and K. Lindenberg, Phys. Rev. E **71**, 051906 (2005).
[10] R. Reigada, J. Buceta, and K. Lindenberg, Phys. Rev. E **72**, 051921 (2005).
[11] K. Simons and E. Ikonen, Nature (London) **387**, 569 (1997).
[12] K. Simons and D. Toomre, Nat. Rev. Mol. Cell. Biol. **1**, 31 (2000).
[13] A. D. Douglass and R. D. Vale, Cell **121**, 937 (2005).
[14] J. R. Silvius, Biochim. Biophys. Acta **1610**, 174 (2003).
[15] R. Reigada, J. Buceta, J. Gómez, F. Sagués, and K. Lindenberg, J. Chem. Phys. **128**, 025102 (2008).
[16] S. Mayor and M. Rao, Traffic (Oxford, U. K.) **5**, 231 (2004).
[17] P. Sharma, R. Varma, R. C. Sarasij, K. Gousset, G. Krishnamoorthy, M. Rao, and S. Mayor, Cell **116**, 577 (2004).
[18] W. K. Subczynski and A. Kusumi, Biochim. Biophys. Acta **1610**, 231 (2003).

[19] L. Foret, Europhys. Lett. **71**, 508 (2005).
[20] M. S. Turner, P. Sens, and N. D. Socci, Phys. Rev. Lett. **95**, 168301 (2005).
[21] J. Gómez, F. Sagués, and R. Reigada, Phys. Rev. E **77**, 021907 (2008).
[22] J. W. Cahn and J. E. Hilliard, J. Chem. Phys. **28**, 258 (1958).
[23] C. H. P. Lupis, *Chemical Thermodynamics of Materials* (Elsevier, Amsterdam, 1983).
[24] P. F. F. Almeida, A. Pokorny, and A. Hinderliter, Biochim. Biophys. Acta **1720**, 1 (2005).
[25] M. L. Frazier, J. R. Wright, A. Pokorny, and P. F. F. Almeida, Biophys. J. **92**, 2422 (2007).
[26] M. D. Houslay and K. K. Stanley, *Dynamics of Biological Membranes* (Wiley, New York, 1982).
[27] See EPAPS Document No. E-PLEEE8-80-036907 for a movie file showing the dynamic adaptation of a simulated 256 $\times$256 system subjected to changes in the recycling frequency (rec. freq.). The other parameters are $\bar{\phi}=-0.2$, $\bar{c}=0.214$, $D=1$, $\gamma=0.25$, $J=0.25$, and $G=2.5$. Each snapshot corresponds to a red scale representation of the parameter ϕ (left) and c (right). Red regions correspond to higher values of the represented variables. For more information on EPAPS, see http://www.aip.org/pubservs/epaps.html.
[28] O. Carrillo, M. A. Santos, J. García-Ojalvo, and J. M. Sancho, Europhys. Lett. **65**, 452 (2004).
[29] G. W. Feigenson and J. T. Bulboltz, Biophys. J. **80**, 2775 (2001).
[30] S. L. Veatch, O. Soubias, S. L. Keller, and K. Gawrisch, Proc. Natl. Acad. Sci. U.S.A. **104**, 17650 (2007).
[31] K. Simons and E. Ikonen, Science **290**, 1721 (2000).
[32] T. L. Steck, J. Ye, and Y. Lange, Biophys. J. **83**, 2118 (2002).
[33] A. Kusumi, I. Koyama-Honda, and K. Suzuki, Traffic (Oxford, U. K.) **5**, 213 (2004).
[34] J. F. Hancock, Nat. Rev. Mol. Cell. Biol. **7**, 456 (2006).
[35] M. C. Sabra, H. Gilhøj, and O. G. Mouritsen, Phys. Rev. E **58**, 3547 (1998).
[36] J. R. Henriksen, M. C. Sabra, and O. G. Mouritsen, Phys. Rev. E **62**, 7070 (2000).
[37] M. C. Sabra and O. G. Mouritsen, Biophys. J. **74**, 745 (1998).